NIRSpec detectors: noise properties and the effect of signal dependent inter-pixel crosstalk

Giovanna Giardino[a], Marco Sirianni[a], Stephan M. Birkmann[a] , Bernard J. Rauscher[c] , Don Lindler[c], Torsten Boeker[a] , Pierre Ferruit[a] , Guido De Marchi[a] , Martin Stuhlinger[b], Peter Jensen[b] , Paolo Strada[b]

[a]European Space Agency, ESTEC, Keplerlaan 1 2200AG Noordwijk, The Netherlands;
[b]European Space Agency, ESAC, P.O. Box 78, Villanueva de la Canñada, Spain;
[c]NASA's Goddard SPace Flight Center, Mail Code 130, Greenbelt, MD 20771 USA

ABSTRACT

NIRSpec (Near Infrared Spectrograph) is one of the four science instruments of the James Webb Space Telescope (JWST) and its focal plane consists of two HAWAII-2RG sensors operating in the wavelength range $0.6-5.0\mu$m. As part of characterizing NIRSpec, we studied the noise properties of these detectors under dark and illuminated conditions. Under dark conditions, and as already known, 1/f noise in the detector system produces somewhat more noise than can be accounted for by a simple model that includes white read noise and shot noise on integrated charge. More surprisingly, at high flux, we observe significantly lower total noise levels than expected. We show this effect to be due to pixel-to-pixel correlations introduced by signal dependent inter-pixel crosstalk, with an inter-pixel coupling factor, α, that ranges from ~ 0.01 for zero signal to ~ 0.03 close to saturation.

Keywords: JWST, NIRSpec, Near Infrared Detectors, Noise, Crosstalk

1. INTRODUCTION

NIRSpec (Near Infrared Spectrograph) is a near-infrared multi-object spectrograph and one of the four science instruments of the James Webb Space Telescope (JWST). NIRSpec is being developed by the European Space Agency (ESA) with EADS Astrium Germany GmbH as the prime contractor and it will be the first slit-based astronomical multi-object spectrograph (MOS) to fly in space. A selectable $3'' \times 3''$ integral field unit (IFU) and five fixed slits are also available for detailed spectroscopic studies of single objects.

All three NIRSpec modes (MOS, IFU, and fixed slits) share the need for large-format, high quantum efficiency, and ultra low-noise detectors covering the $\lambda = 0.6-5$ μm spectral range. This need is fulfilled by two 2048×2048 pixel, 5.3 μm cutoff ($\lambda_{\rm co} = 5.3\mu$m), Teledyne HAWAII-2RG (H2RG) sensor chip assemblies (SCAs), with 18 μm pixel pitch. HAWAII-2RG is short for HgCdTe Astronomy Wide Area Infrared Imager with Reference pixels and Guide mode (see Beletic *et al.*[1] for more details on these detectors). These IR sensors are hybrid CMOS (complementary metal-oxide-semiconductor) arrays, with HgCdTe used for light detection and a silicon integrated circuit for signal readout. Similar detectors will be used by the other near-IR instruments on board JWST (NIRCam and NIRISS) and on board of the future ESA mission, EUCLID.[2] They are also currently being used in instruments of ground facilities such as the Near Infrared Integral Field Spectrograph at Gemini North at Mauna Kea (Hawaii) or X-shooter at the European Souther Observatory at Paranal (Chile), and similar HAWAII-1R detectors are in use in Hubble Space Telescope Wild Field Camera 3.

This paper describes the overall noise properties of the two detector arrays (SCA491 and SCA492) in NIRSpec focal plane FPA 104 and provides insights into some non-ideal behaviors that have been observed in these early flight model NIRSpec detectors. In particular, one finding that we report here is the presence, for high signal levels, of signal dependent inter-pixel crosstalk.

Further author information: (Send correspondence to G.G.)
G.G.: E-mail: giovanna.giardino@esa.int, Telephone: +31 71 565 4625
M.S.: E-mail: marco.sirianni@esa.int, Telephone: +31 71 565

High Energy, Optical, and Infrared Detectors for Astronomy V, edited by Andrew D. Holland, James W. Beletic,
Proc. of SPIE Vol. 8453, 84531T · © 2012 SPIE · CCC code: 0277-786X/12/$18 · doi: 10.1117/12.925357

2. NIRSPEC DETECTORS

JWST's H2RG detectors[1,3] achieve very low dark currents (< 0.01 e$^-$s^{-1}pixel^{-1}) and high quantum efficiency (80-90%) over a wide bandpass.[4] The two H2RG SCAs for NIRSpec focal plane, together with the two application-specific integrated circuits (ASICs) that control them, were delivered to ESA, integrated and characterized, by the NIRSpec Detector Subsystem team of Goddard Space Flight Center in the fall of 2010, together with the detector system (DS) test data set.

For most science observations, NIRSpec detectors acquire up-the-ramp sampled data at a constant cadence of one frame every 10.73 s. A frame is the unit of data that results from sequentially clocking through and reading out a rectangular area of pixels. Most often, this will be all of the pixels in the SCA, although smaller sub-arrays are also possible when faster cadences are needed to observe, e.g., bright targets. Following HST-NICMOS, we have dubbed this readout pattern MULTIACCUM, frequently abbreviated as MULTI-$n \times m$, where n is the number of equally spaced groups sampling up the ramp, and m is the number of averaged frames per group. In the idealized situation where the only noise components are white readout noise and shot noise on integrated charge, NIRSpec total noise scales with MULTIACCUM readout pattern according to the expression:[5–7]

$$\sigma^2_{\rm total} = \frac{12(n-1)}{mn(n+1)}\sigma^2_{\rm read} + \frac{6(n^2+1)}{5n(n+1)}(n-1)t_g f - \frac{2(m^2-1)(n-1)}{mn(n+1)}(m-1)t_f f\,. \quad (1)$$

In this formula, $\sigma_{\rm total}$ is the total noise in units of e$^-$ rms, $\sigma_{\rm read}$ is the read noise per frame in units of e$^-$ rms, and f is flux in units of e$^-$s^{-1}pixel^{-1}, where f includes photonic current and dark current. The noise model includes read noise and shot noise on integrated flux, which is correlated across the multiple non-destructive reads sampling up the ramp. For the special case of dark integrations, $f = i_{\rm dark}$.

To characterize the total noise of our detectors and compare it to the theoretical expectation using Eq. 1, we selected dark and flat exposures out of the DS tests data set.

3. TOTAL NOISE OF NIRSPEC DETECTORS

The subset of DS test data that we processed and analyzed consists of 100 dark exposures, 50 flat exposures at a "low" flux level of $f \sim 1.2$ e$^-$s^{-1}pixel^{-1}, and 25 exposures at a high flux level of $f \sim 150$ e$^-$s^{-1}pixel^{-1}. The darks and high flux exposures were taken with a MULTI-88 $\times$ 1 readout pattern (thus $n = 88$ and $m = 1$), whereas for the low flux exposures only 10 groups up-the-ramp were acquired (thus $n = 10$ and $m = 1$). In our case $t_g = t_f = 10.73$ s.

To compute the expected total noise using Eq. 1 a measure of the detector read noise is necessary. As discussed in Rauscher *et al.*,[5] under ultra low photon flux and ultra low dark current conditions, $\sigma_{\rm read} \approx \sigma_{\rm CDS}/\sqrt{2}$, where CDS stands for "Correlated Double Sampling". This means that we can estimate the read noise variance from the variance of the difference of two adjacent groups in dark exposures. From two (arbitrarily chosen) dark exposures a data-cube containing 88 independent differences of 2 adjacent groups was constructed; the standard deviation (SD), with iterative 3σ-rejection, over these 88 images was then computed, for each pixel, providing a map of $\sigma_{\rm CDS}$, from which a map of $\sigma_{\rm read}$ is readily derived. As summarized in Table 1, the typical value of $\sigma_{\rm read}$ for our detectors is ~ 12 e$^-$.

To compute the total noise each exposure MULTIACCUM cube was first processed to derive the count-rate image. This involves the following steps: bias subtraction, reference pixel subtraction, linearity correction, and up-the ramp fitting to derive the count rate (see Birkmann[8] and Boeker *et al.*[9] for a more detailed description of our pipeline). In addition, the step of Inter Pixel Capacitance (IPC) correction can be optionally applied before that of linearity correction, and in the following description of the data analysis, if the step of IPC correction was applied, we will explicitly state it. For this step, the IPC coupling values as characterized by the NIRSpec DS team were used (see next section). Our processing pipeline has the option of performing optimal up-the ramp fitting using pre-defined weights as prescribed in the algorithm described by Fixsen *et al.*[10] or simply using a linear least squared straight line fit to the data and determine the slope. Although non-optimal in terms of signal-to-noise, for the purpose of this exercise we opted for the linear least squared fit option, for which Eq. 1 applies.

Table 1. Median value of the total noise for the two H2RG SCAs in NIRSpec focal plane, for different levels of illumination, compared with prediction from Eq. 1. The median values of the read noise (as derived from CDS noise)are also given. Values are in e^-.

	SCA491		SCA492	
	Data	Eq. 1	Data	Eq. 1
Darks	7.2	5.5	6.5	5.2
Low flux ($f \sim 1.2$ e^-s^{-1})	17.8	17.0	16.8	16.1
Low flux ($f \sim 1.2$ e^-s^{-1}) - IPC corrected	18.4	17.1	17.5	16.1
High flux ($f \sim 150$ e^-s^{-1})	271.6	312.6	266.0	307.1
High flux ($f \sim 150$ e^-s^{-1}) - IPC corrected	277.3	312.7	277.4	307.1
Read Noise	12.6		11. 9	

All exposures for a given level of illumination were then combined to derive a map of the mean count-rate and a map of the SD (in e^-s^{-1}) for that illumination. The SD map multiplied for the exposure integration time, $t_{\rm int} = (n-1)t_g$, provides a map of the total noise. The median values of the total noise distribution across the entire detector array are given in Table 1 for the darks and the two levels of incident flux. The measured values are compared in Table 1 with the expected noise level computed using Eq. 1. These are also the median values of the distribution (across the array) of the expected total noise, derived from Eq. 1, using the $\sigma_{\rm read}$-map and the mean count-rate map (as f) for a given data set.

As shown in Table 1 the observed total noise in dark exposures is $\sim 25\%$ higher than predicted for an ideal detector with the same read noise (as derived from CDS noise). Moseley *et al.*[11] have carried out a principal component analysis of the read-noise of these detectors and found it to be dominated by a component with a 1/f spectrum. This component is not fully characterized by the CDS noise, therefore explaining the discrepancy between predicted and observed total noise in this case. Indeed one can use Eq. 1 to estimate the value of an effective read-noise, defined as the value of $\sigma_{\rm read}$ required for the computed total noise to match the observed value. This is ~ 18 e^- (for a MULTI-88 $\times$ 1 exposure*).

At low flux levels, the measured median total noise values are in better agreement with the values computed from Eq. 1, using the same $\sigma_{\rm read}$ map used for the darks and, as f, the mean count-rate map for these exposures (cf. Table 1). The presence of IPC in these detectors, however, has the effect of spuriously lowering the observed noise level compared to the prediction of Eq. 1. Due to IPC, charge that is accumulated in one pixel is partly detected in the 4-neighboring pixels (at the level of $\sim 1\%$ per each 4-neighbor), thereby introducing a correlation among the signal of adjacent pixels. We investigated this effect by applying IPC correction when processing all the 50 'low flux' exposures and generating from these new mean flux and total noise maps. As shown in Table 1, correcting for IPC leads to a $3-4\%$ higher noise level and hence to a higher discrepancy between predicted and measured values. This discrepancy, however, can be explained in terms of the 1/f-read noise component not accounted for by the CDS noise. Indeed, by substituting in Eq. 1 the effective read-noise value for a MULTI-10 $\times$ 1 exposures (which is ~ 14 e^-), one finds that the computed median total noise value agrees well with that measured from the IPC-corrected exposures.

At high flux level ($f \sim 150$ $e^-s^{-1}pixel^{-1}$) the comparison between computed and measured total noise is more surprising, as can be seen from Table 1; the measured total noise of the real detector appears to be $\sim 15\%$ lower than that for an ideal system, as computed from Eq. 1 (using the mean count-rate map for these exposures as f and the same $\sigma_{\rm read}$ map used for the darks). Correction for IPC reduces this discrepancy only marginally. At these flux levels, the total noise of the exposure is completely dominated by the poissonian fluctuations in the photon field. This component is expressed in Eq. 1 by the second and third term – the latter, however, is

*The effective read-noise to be used for Eq. 1 to match the measured value depends on the number of groups in the dark exposures, the longer the exposure the higher the effective $\sigma_{\rm read}$ value, as the effects of the 1/f-read noise component accumulates.

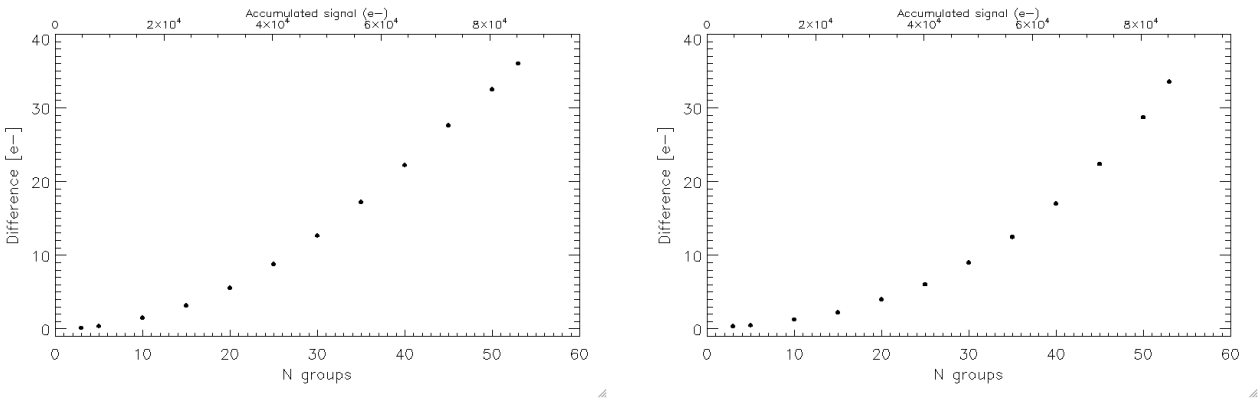

Figure 1. Difference between the total noise level predicted using Eq. 1 and the observed value, as a function of the number of groups used to derive the count-rate image in each of the 25 high-flux exposures, for the two NIRSpec detectors. At this flux level ($f \sim 150$ e$^-$s^{-1}) most pixel reach saturation by group 53.

0 in our case, because $m = 1$ – that evaluate the total noise component coming from the poissonian statistics of the incident photons, taking into account the signal correlation of the up-the-ramp fitting. We note, though, that even by taking the simple poissonian noise of the total number of accumulated counts, one derives an (under-)estimate of the total noise of ~ 290 e$^-$, which is however still higher than the observed total noise.

We investigated whether the discrepancy between observed and predicted noise was dependent on the signal accumulated in the pixel potential well by looking at the difference between predicted noise levels and measured ones, as a function of the number of groups used to derive each exposure count-rate. Note that, although these exposures were acquired with MULTI-88 $\times$ 1 pattern, at this flux level, most pixels reach saturation by $n = 53$[†]

As shown in Fig. 1, indeed, the difference between the noise level theoretically expected and the one observed by computing the STD of the count-rate across the 25 high-flux exposures increases steadily with the number of groups (that is with the signal accumulated in the pixels), reaching the maximum level close to the pixel full well capacity.

4. ADDITIONAL PIXEL-TO-PIXEL CORRELATION

An obvious interpretation for the noise 'deficiency' observed at high counts could be the presence of extra inter-pixel correlation on top of the known IPC level, for which we can correct for.

For the purpose of characterizing the magnitude of inter-pixel crosstalk, and following Moore *et al.*,[12] charge appearing electrically in surrounding pixels can be described in terms of a single variable α, defined as the percent of total charge seen in any of the four nearest neighbor pixels. In other words, neglecting "second neighbor" and "diagonal neighbor" coupling and assuming two-dimensional symmetry in nearest neighboring pixels, the center node loses 4α of its charge – 1α to each of its four nearest neighbors. This can also be represented in terms of a 3×3 impulse-response array as:

$$K = \begin{pmatrix} 0 & \alpha & 0 \\ \alpha & 1-4\alpha & \alpha \\ 0 & \alpha & 0 \end{pmatrix} \tag{2}$$

The IPC for these detector was characterized by the NIRSpec DS team using a variety of methods: hot-pixels, cosmic-ray events (CRE) and noise correlation matrix.[12] All the three methods gave consistent results, with $\alpha \sim 0.01$, for both SCAs. They also allow a median 3×3-array to be derived representing the IPC-coupling to the central pixel, for each SCA output, and these arrays are those used by our pipeline to deconvolve each

[†]When computing the expected noise level for each individual pixel, the number of groups used by the pipeline to derive the count-rate in that pixel is being used in Eq. 1

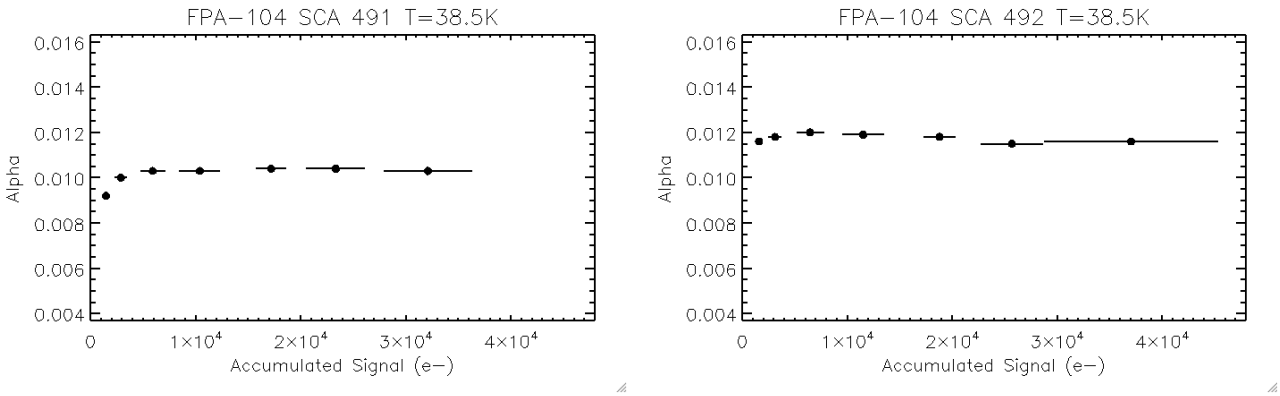

Figure 2. The value of the pixel-to-pixel coupling coefficient α as derived from the analysis of 4-neighbors of hot-pixels, as a function of the signal in the hot-pixel – see text.

frame for the known IPC effect. All these three methods, however, sampled signal levels only up to $\sim 12,000\ e^-$, while as shown in Fig. 1 the discrepancy that we observe between predicted and observed total noise starts to be significant when using exposures with at least 15 groups, which at a flux of $\sim 150\ \mathrm{e^-s^{-1}}$, corresponds to integrated signals of $\sim 25,000\ \mathrm{e^-}$.

To explore the hypothesis that the noise 'deficiency' observed at high counts could be due to an increasing level of inter-pixel crosstalk somehow dependent on the pixel accumulated electrical signal we extended the analysis of the pixel crosstalk using hot-pixels with signals up to $\sim 45,000$ counts. From multiple dark exposures we created a high signal-to-noise up the ramp cube, where isolated hot pixels with no neighbor within 5 pixels were identified. Regions 3×3-pixel in size were extracted around each isolated hot pixel, background subtracted, and normalized by the value of the hot pixel. All selected hot pixel were then grouped in bins of increasing accumulated signal, with each bin including between few hundreds to few thousands pixels. Median values of the 3×3 regions over all hot pixels within a given bin of accumulated signal were calculated and used to derive the value of α. The result of this analysis is shown in Fig. 2: the value of α appears to be overall constant across a large range of accumulated signal.

Note, however, that in hot-pixels the signal is not due to photon-generated charges but to defects or impurities in the crystal lattice. Thus, to test the possibility that additional inter-pixel crosstalk could be somehow depend on the level of photon-generated charge collected by a pixel, we computed the noise auto-correlation of different frames in the high-flux set of exposures. This was done according to the following procedure: *i*) for each integration, the entire integration cube is processed to obtain an exposure cube where each frames is reference pixel subtracted and each pixel integration ramp is corrected for the non-linearity effect and eventually for the IPC effect; *ii*) for each pair of exposure a CDS difference between group n and group 0 was computed and the difference of the two CDS images is taken to construct a noise image with the signal removed: noise_n = CDS2(n) − CDS1(n); *iii*) The auto-correlation (c) is computed over all pixels (x,y) that have no inoperable pixel within a neighborhood of 3 pixels [‡] as

$$c_n(i,j) = (1/c_n(0,0)) \sum_{xy} \mathrm{noise}_n[x,y] \cdot \mathrm{noise}_n[x+i, y+j], \quad i,j \in [0,3]$$

iv) the final correlation matrix for group n is taken to be the median of all correlation matrix computed from all independent pairs of observations (12 pair in total), for that group.

The value of α (for small values of α) is approximated by:

$$b = [c(1,0) + c(0,1)]\,/2$$

[‡]where an inoperable pixel is defined to a pixel having dark total noise $> 12\mathrm{e^-}$ and differential quantum efficiency (DQE) $< 70\%$ of the average DQE

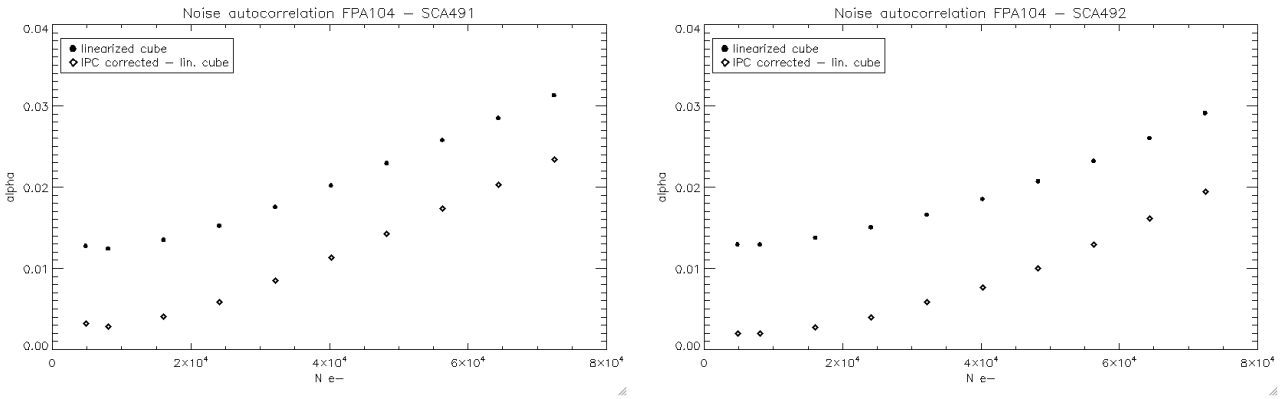

Figure 3. The value of the pixel-to-pixel correlation coefficient α as derived from the noise auto-correlation matrix as a function of the signal accumulated in the pixel potential well.

$$\alpha = b/2 - b^2.$$

The value of α was computed in this way for $n = (3, 5, 10, 15, .., 40, 45)$ for both SCAs, with and without applying IPC correction. The results are plotted in Fig. 3 as a function of the number of electron, N_{e^-}, accumulated at each group n for which the auto-correlation matrix was derived ($N_{\mathrm{e}^-} = n \cdot t_g \cdot f$), the two curves in each plot corresponding to the cases with and without IPC correction.

After an initial plateau for $N_{e^-} < 20,000$, where $\alpha \sim 0.012$ (or 0.002 when IPC correction is applied), the value of α increases gradually to reach a maximum of ~ 0.03 at $N_{e^-} \sim 75,000$ (n=45). We note, that even at very low signals, the value of α derived here, is somewhat higher than the value derived from the IPC analysis using the hot-pixels and cosmic-ray method or the noise autocorrelation method (in other words, even when the IPC correction is applied the value α at low signals in the plots is not ~ 0). This is because, unlike the analysis conducted for IPC with hot-pixels and cosmic-ray hits or using the noise auto-correlation matrix without applying linearity correction, an extra step of bias subtraction was applied here, which is introducing an additional small constant correlation term (due to the residual 1/f-read noise component present in the bias).

The plots in Fig. 3 clearly confirms the presence for N_{e^-} greater than $\sim 20,000$ of an additional inter-pixel crosstalk term, which increases with the number of photon-generated charges collected in the pixels, reaching, near the pixel saturation point, a coupling value α of about three times the IPC value as derived from hot pixels (in dark exposures). This signal-dependent pixel-to-pixel crosstalk explains the discrepancy between predicted and observed total-noise discussed in the previous section. Indeed we have verified by Monte Carlo simulations that the values of α derived here are the values required to explain the observed level of total noise.

4.1 The edge effect of signal-dependent inter-pixel crosstalk

Another effect of this additional, signal dependent, inter-pixel crosstalk term is to modify the shape of the edge of high contrast sources. In other words, the point- or slit-spread function of bright-sources widens as the source counts accumulates. We came across this effect during the first cycle of NIRSpec Calibration and Performance Verification campaign. Our Radiometric-Calibrated Spectral Source (RCSS) had a point-spread function with wider wings than expected and their relative size increased with the intensity of the RCCS lamp. In addition, the integration ramps of the pixels within these wings had an anomalous shape similar to those shown in the left panel of Fig. 4.

The figure displays the integration ramps at the edge of a dispersed image from NIRSpec fat-slit. A strong lamp was used in this case, with a constant count-rate of ~ 620 e^-/s. Although corrected for non-linearity, the ramps are not straight and as we move away from the inside to the outside of the slit, the ramps display a pronounce bend, in the opposite direction of the pixel non-linear behavior, as if the the illumination rate increased with time. It is easy to see how this effect can be explained in terms of coupling among adjacent pixels

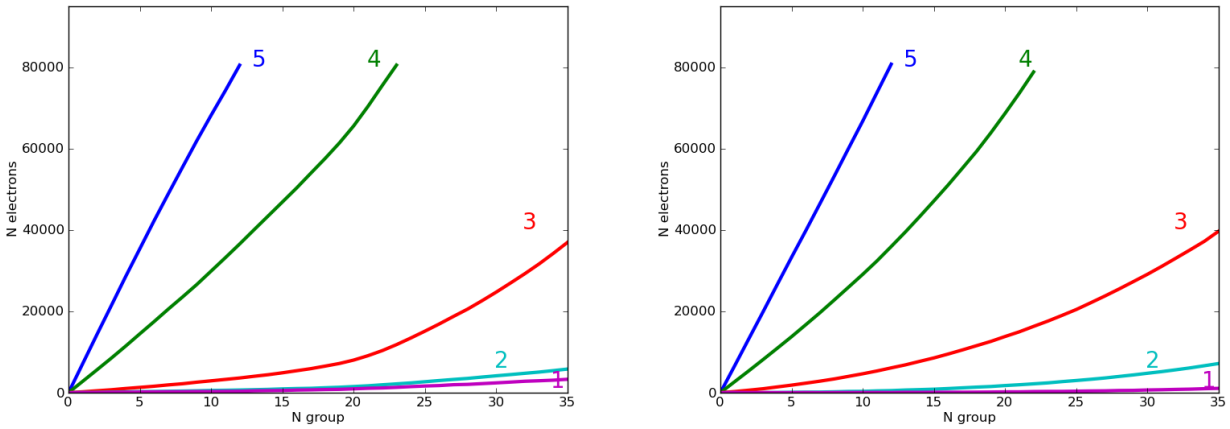

Figure 4. The effect of signal-dependent inter-pixel cross talk on the integration ramps of pixels at the edge of a bright source. The left panel shows the anomalous shapes of the integration ramps from pixels at the edge of a dispersed image of NIRSpec fat-slit, the right panel refer to simulated data where the effect of signal-dependent crosstalk was incorporated (see text). The group of pixels from where the ramps were extracted, in the real data and in the simulations, are shown in Fig. 5, below, in the left and right panel, respectively.

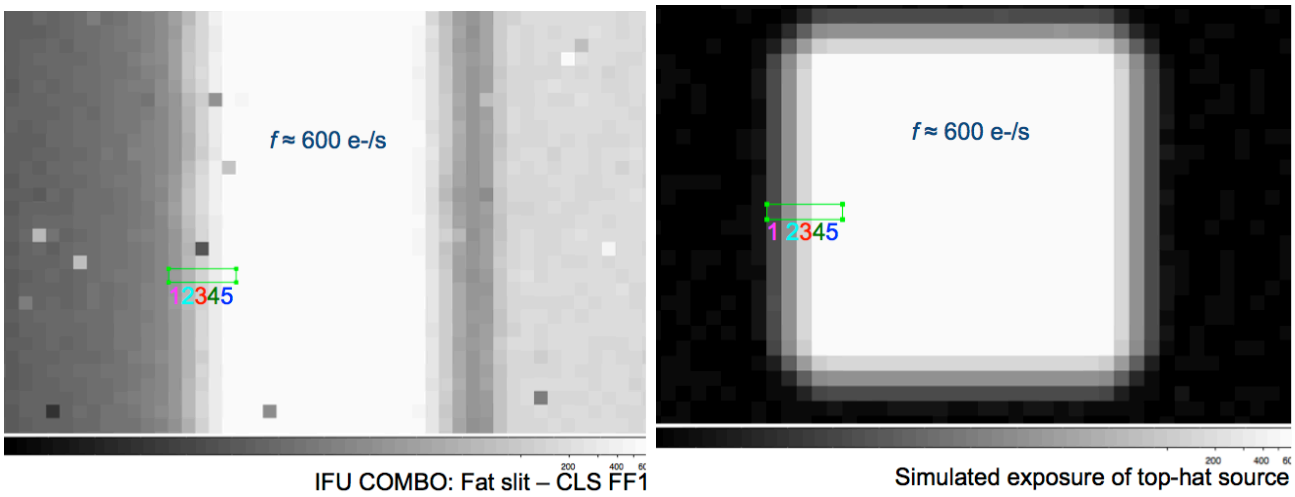

Figure 5. Zoom-in onto the count-rate image of NIRSpec fat slit illuminated by a strong dispersed source (right panel) and onto the count-rate image of a simulated exposures of a top-hat source with similar intensity. The simulation incorporated the effect of the signal-dependent inter-pixel crosstalk term (see text). The rectangles indicate the pixels from where the anomalous integration ramps shown in Fig. 4 were extracted.

which increases with the level of accumulated signal. The right panel of Fig. 4 shows the ramps from the edge of a simulated observation of a top-hat source with $f \sim 620$ e$^-$/s.

In the simulation the effect of the signal-dependent crosstalk was simulated in each frame of the integration by convolving a pixel accumulated signal with a kernel of the type given in Eq. 2, with the value of α taken to be that given by the curve in Fig. 3 (linearly interpolated) for that particular level of accumulated charge (for SCA491, which is the detector-array were the fat slit spectrum falls in this case). For the rest, the simulation of the NIRSpec exposure was very simplistic, incorporating only white read-noise, dark-currents and poissonian noise. The top-hat source has a "smooth" edge roughly reproducing the intrinsic slit spread function of NIRSpec fat-slit.

Although the simulation was quite simplistic, the general shape of the anomalous ramps are reproduced in the simulated data. In the simulated exposure, the only non-ideal process is the presence of signal-dependent pixel-to-pixel coupling, so the similarity between real and simulated edge-ramps is consistent with signal-dependent crosstalk being at the origin of their anomalous shape.

5. DISCUSSION AND CONCLUSIONS

In these detectors, crosstalk between pixels can be caused by two independent phenomena, IPC, and charge diffusion. IPC is the capacitance that arises between adjacent detector pixels in the source-follower CMOS design, and leads to coupling of signal between those pixels via displacement currents flowing from the collection node. Charge diffusion is the lateral movement (pixel-to-pixel) of charge between the points of charge production and charge collection in the bulk of the detector. While charge diffusion is a stochastic process and therefore obeys Poissonian statistics, IPC is a deterministic process that leads to noise correlation and hence to pixel displaying 'sub-poissonian' noise.[12,13] As described in the previous section, at high illumination levels, our detectors appear to have sub-poissonian noise levels and displays signal dependent noise correlations thus ruling out charge diffusion as a major contribution to the observed pixel-to-pixel coupling and indicating that we are dominated by an IPC-type of crosstalk.

The dependency of the IPC effect with accumulated charge has been only very limitedly studied so far. Cheng[14] studied the dependency with temperature and accumulated charge of the IPC effect in hybrid HgCdTe. In his study, IPC coupling as measured from hot-pixels and CRE in dark exposures initially decreases with accumulated counts from $\sim$ 0.02 to approximately 0.01 at 5,000 ADUs (Analog-to-Digital Units) but then stays roughly constant up to 30,000 ADUs. Conversely, when looking at CRE in illuminated exposures (flat illuminations), Cheng[14] finds that the IPC coupling appears to increase from 0.01 to $\sim$ 0.03. Apart from the initial drop in coupling value when using hot-pixel, his findings are in agreement with our results. We also see the α value being overall constant with the accumulated signal when looking at the coupling between hot-pixels and its neighbors in dark exposures, while α clearly increases with the pixel accumulated charge, when looking at the noise correlation in intensely illuminated exposures.

In the model of IPC developed by Moore et al.,[12] the detector array of photodiodes is represented as an array of capacitors, each with identical capacitance, and the IPC coupling is represented by small coupling capacitors between the nodes. The inter-pixel coupling depends on the relative value of the node capacitance and the coupling capacitance. Since in these detectors the node capacitance increases as a function of voltage (i.e. as a function of accumulated charge), but the cross-coupling capacitance is independent of the voltage (at least for the most part), one would indeed expect α to increase with signal, as we see in our cross-correlation measurements. Nevertheless, this does not explain the fact that α measurements using hot pixels in dark exposures shows α to be constant across a large range of accumulated charge, unless the leakage current from the hot pixel somehow modifies the behavior of the neighboring capacitors.

From a phenomenological point of view, if this signal dependent inter-pixel cross talk is indeed an IPC effect, one would expect its intensity to be independent from the wavelength of the incident photons. Following the noise autocorrelation approach described in Sect. 4, we have derived the value of α as a function of wavelength using the monochromatic flat fields acquired during the DS tests for Quantum Efficiency characterization. In this case, the flux is very strong; at 2.6 μm, $f \sim 930$ e$^-$/s, so that only 5 groups were acquired per exposures. Fig. 6 shows the value of α as a function of wavelength, as derived from the noise correlation matrix computed for group 3 and 5 in these exposures (only a pair of exposure at each wavelength was used in this case). Also in this case the value of α increases with accumulated charge, i.e. with the number of groups. Below 1.6 μm, α increases steeply with wavelength, however, at these wavelengths, the detector quantum yield becomes greater than one. As shown by McCullough *et al.*[15] and Fox *et al.*,[16] in this type of detectors, the quantum yield exceeds unity for $\lambda < 0.28\lambda_{co} \approx 1.5$ μm. This means that, for λ lower than 1.6 μm, we are facing multiple charge generation for each incident photon, that leads to further pixel-to-pixel correlation. Therefore we cannot easily say what is the dependency of the signal-dependent crosstalk term with wavelength, in this range. From 1.6 to 5μm, however, the value of α appears to be essentially independent from wavelength, consistent with this inter-pixel crosstalk term being generated by an IPC-type effect.

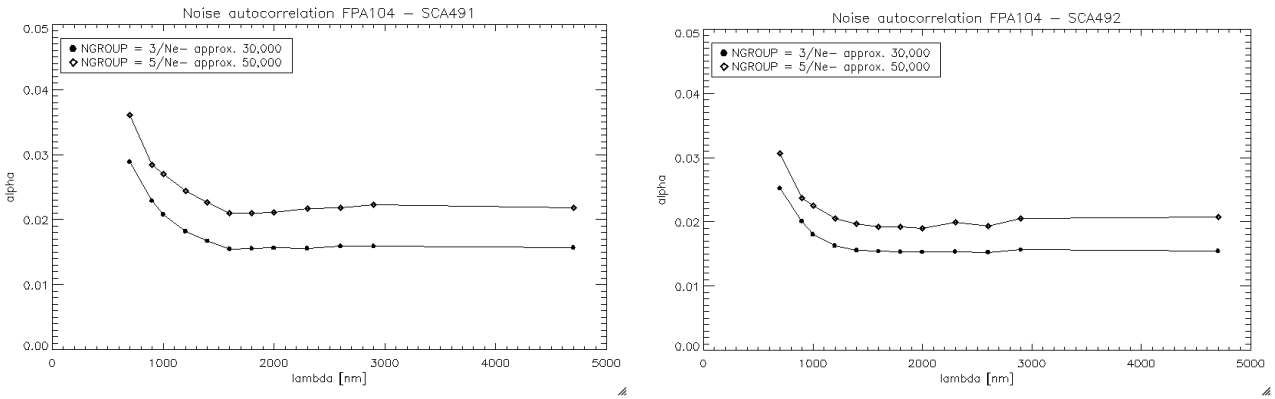

Figure 6. The dependency of α with wavelength as derived from the noise autocorrelation matrix of monochromatic flat flats. The quantum yield exceeds unity for λ lower then ~ 1.4 μm.

In summary, we have reported here of the presence, in NIRSpec two H2RG detector arrays, of deterministic inter-pixel crosstalk which increases with the pixel accumulated charge. This effect is significant, reaching a coupling of 3% near pixel full well, in other words, for $N_e > 45,000$ a pixel will be 'leaking' more than 10% of the detected signal to its neighboring pixels. This has the consequence of degrading (widening) the point and slit spread function of strong sources.

The evidence from this study is that this crosstalk term is likely linked to the IPC effect, however a proper explanation needs to provide the reason of its different behavior in the case of dark and illuminated exposures. To improve the characterization of this crosstalk term, we plan to acquire specific data during the upcoming Cycle 2 of NIRSpec Calibration and Performance Verification campaign[17]) and to develop a quantitative model of this effect.

ACKNOWLEDGMENTS

We thank Samuel Harvey Moseley and Markus Loose for very useful discussions.

REFERENCES

[1] Beletic, J. W., Blank, R., Gulbransen, D., et al., "Teledyne Imaging Sensors: infrared imaging technologies for astronomy and civil space," in [*Society of Photo-Optical Instrumentation Engineers (SPIE) Conference Series*], *Society of Photo-Optical Instrumentation Engineers (SPIE) Conference Series* **7021** (Aug. 2008).

[2] Laureijs, R. J., Duvet, L., Escudero Sanz, I., et al., "The Euclid Mission," in [*Society of Photo-Optical Instrumentation Engineers (SPIE) Conference Series*], *Society of Photo-Optical Instrumentation Engineers (SPIE) Conference Series* **7731** (July 2010).

[3] Loose, M., Beletic, J., Garnett, J., and Xu, M., "High-performance focal plane arrays based on the HAWAII-2RG/4G and the SIDECAR ASIC," in [*Society of Photo-Optical Instrumentation Engineers (SPIE) Conference Series*], *Society of Photo-Optical Instrumentation Engineers (SPIE) Conference Series* **6690** (Sept. 2007).

[4] Rauscher, B. J., Alexander, D., Brambora, C. K., et al., "James Webb Space Telescope Near-Infrared Spectrograph: dark performance of the first flight candidate detector arrays," in [*Society of Photo-Optical Instrumentation Engineers (SPIE) Conference Series*], *Society of Photo-Optical Instrumentation Engineers (SPIE) Conference Series* **7021** (Aug. 2008).

[5] Rauscher, B. J., Fox, O., Ferruit, P., et al., "Detectors for the James Webb Space Telescope Near-Infrared Spectrograph. I. Readout Mode, Noise Model, and Calibration Considerations," *PASP* **119**, 768–786 (July 2007).

[6] Rauscher, B. J., Fox, O., Ferruit, P., et al., "Erratum," *PASP* **122**, 1254 (Erratum) (2010).

[7] Rauscher, B. J., Arendt, R. G., Fixsen, et al., "Reducing the read noise of HAWAII-2RG based detector systems with improved reference sampling and subtraction (IRS^2)," *Proc SPIE* **8155**, 45 (Sept. 2011).

[8] Birkmann, S., "Description of the NIRSpec pre-processing pipeline," NIRSpec Technical Note NTN-2011-004, ESA/ESTEC available at http://www.rssd.esa.int/index.php?project=JWST (2011).

[9] Boeker, T., Birkmann, S., De Marchi, G., et al., "The spectro-photometric calibration of the JWST NIRSpec instrument," in [*Society of Photo-Optical Instrumentation Engineers (SPIE) Conference Series*], **Paper No. 8442-124** (This conference).

[10] Fixsen, D. J., Offenberg, J. D., Hanisch, R. J., et al., "Cosmic-Ray Rejection and Readout Efficiency for Large-Area Arrays," *PASP* **112**, 1350–1359 (Oct. 2000).

[11] Moseley, S. H., Arendt, R. G., Fixsen, D. J., et al., "Reducing the read noise of H2RG detector arrays: eliminating correlated noise with efficient use of reference signals," in [*Society of Photo-Optical Instrumentation Engineers (SPIE) Conference Series*], *Society of Photo-Optical Instrumentation Engineers (SPIE) Conference Series* **7742** (July 2010).

[12] Moore, A. C., Ninkov, Z., and Forrest, W. J., "Interpixel capacitance in nondestructive focal plane arrays," in [*Society of Photo-Optical Instrumentation Engineers (SPIE) Conference Series*], Grycewicz, T. J. and McCreight, C. R., eds., *Society of Photo-Optical Instrumentation Engineers (SPIE) Conference Series* **5167**, 204–215 (Jan. 2004).

[13] Moore, A. C., Ninkov, Z., and Forrest, W. J., "QE Overestimation and Deterministic Crosstalk Resulting from Inter-pixel Capacitance," *Optical Engineering* **46**, 7 (2006).

[14] Cheng, L., *Interpixel Capacitive Coupling*, Master's thesis, Center for Imaging Science - Rochester Institute of Technology (2009).

[15] McCullough, P. R., Regan, M., Bergeron, L., and Lindsay, K., "Quantum Efficiency and Quantum Yield of an HgCdTe Infrared Sensor Array," *Publications of the Astronomical Society of the Pacific* **120**, 759 (July 2008).

[16] Fox, O., Waczynski, A., Wen, Y., Foltz, R. D., Hill, R. J., Kimble, R. A., Malumuth, E., and Rauscher, B. J., "The Fe 55 X-Ray Energy Response of Mercury Cadmium Telluride Near-Infrared Detector Arrays," *Publications of the Astronomical Society of the Pacific* **121**, 743 (July 2009).

[17] Birkmann, S., Boeker, T., , De Marchi, G., et al., "The Near Infrared Spectrograph (NIRSpec) on-ground calibration campaign," in [*Society of Photo-Optical Instrumentation Engineers (SPIE) Conference Series*], **Paper No. 8442-123** (This conference).